EPJ Web of Conferences **94**, 04020 (2015)
DOI: 10.1051/epjconf/20159404020

Mesoscale numerical modeling of plastic bonded explosives under shock loading

Hailin Shang, Feng Zhao[a], Guangfu Ji, and Hua Fu

National Key Laboratory of Shock Wave and Detonation Physics, Institute of Fluid Physics, China Academy of Engineering Physics, Mianyang 621999, Sichuan, China

Abstract. Mesoscale responses of plastic bonded explosives under shock loading are investigated using material point method as implemented in the Uintah Computational Framework. The two-dimensional geometrical model which can approximately reflect the mesoscopic structure of plastic bonded explosives was created based on the Voronoi tessellation. Shock loading for the explosive was performed by a piston moving at a constant velocity. For the purpose of investigating the influence of shock strength on the responses of explosives, two different velocities for the piston were used, 200 m/s and 400 m/s, respectively. The simulation results indicate that under shock loading there forms some stress localizations on the grain boundary of explosive. These stress localizations lead to large plastic deformations, and the plastic strain energy transforms to thermal energy immediately, causing temperature to rise rapidly and form some hot spots on grain boundary areas. The comparison between two different piston velocities shows that with increasing shock strength, the distribution of plastic strain and temperature does not have significant change, but their values increase obviously. Namely, the higher the shock strength is, the higher the hot spot temperature will be.

1. Introduction

Plastic bonded explosives are heterogeneous and often consist of a mixture of polycrystalline explosives and binder materials. Thus, these heterogeneous explosives exhibit obviously different mechanical, thermal and chemical behaviour compared to pure explosives because of the discontinuity at mesoscale which associated with the granular nature of the explosive constituents. Under shock loading, significant temperature and pressure rise at the defect areas of these heterogeneous explosives, forming a lot of hot spots. Thereafter, the chemical reaction and combustion come up, finally the detonation occurs. Because of the difficulties in experimental study at mesoscale, numerical simulation is an available way to investigate the mesoscale response of explosives under shock loading.

Menikoff [1] studied the mechanism for hot-spot formation occurs as a shock wave passes over a high-density impurity using a two-dimensional hydrodynamic simulation performed with the xRage code. The results pointed out that interactions generated by reflected waves from neighboring beads can significantly increase the peak hot-spot temperature when the beads are suitably spaced. Baer [2] studied the mesoscopic processes of consolidation, deformation, and reaction of shocked porous energetic materials using the shock physics code, CTH. Numerical simulations indicate that "hot-spots" are strongly influenced by multiple crystal interactions. Conley et al. [3] investigated the shock compaction in granular porous and cast HMX using a multi-material, two dimensional Eulerian hydrocode, RAVEN. In their simulation results, no significant particle size effect upon HMX temperature was observed in either of the two compacts. But the presence of the binder significantly altered the response of intragranular voids.

In this paper, we studied the shock responses of plastic bonded explosives using material point method as implemented in the Uintah Computational Framework [4].

2. Material point method

The material point method (MPM) was described by Sulsky et al. [5,6] as an extension to the FLIP (Fluid-Implicit Particle) method of Brackbill [7], which itself is an extension of the particle-in-cell (PIC) method of Harlow [8].

The basic idea of MPM is: objects are discretized into particles, or material points, each of which carries the history-dependent state variables such as stresses and strains, as well as mass and kinematic variables such as position, velocity and acceleration [5,9]. A regular background mesh covers the computational domain. The cells of the grid behave like finite elements, and the grid points behave like finite element nodes. During each time step, the mass and kinematic variables at the material points are mapped to the grid, where momentum equations are solved. The acceleration and velocity at the grid are then mapped back to the material points. State variables are then calculated at the material points using the updated kinematic variables.

The use of a regular background grid in MPM has a lot of computational advantages. Computational of spatial gradients is simplified. For heterogeneous materials like explosives, MPM is more suitable for solving problems involving contact between colliding objects, cracks, large

[a] Corresponding author: ifpzf@163.com

deformations and other high velocity problems. It has an advantage over FEM in that the use of the regular grid eliminates the need for doing costly searches for contact surfaces [10].

The discrete momentum equation for MPM is given as:

$$m\mathrm{a} = \mathrm{F}^{\mathrm{ext}} - \mathrm{F}^{\mathrm{int}} \tag{1}$$

where m is the mass matrix, **a** is the acceleration vector, F^{ext} is the external force vector, and $\boldsymbol{F}^{int}$ is the internal force vector resulting from the divergence of the material stresses

The solution begins by accumulating the particle state on the nodes of the computational grid, to form the mass matrix $\boldsymbol{m}$ and to find the nodal external forces $\boldsymbol{F}^{ext}$, and velocities, $\boldsymbol{v}$. These quantities are calculated at individual nodes by the following equations, where $\sum$ represents a summation over all particles:

$$m_i = \sum_p S_{ip} m_p \tag{2}$$

$$\mathrm{v}_i = \frac{\sum_p S_{ip} m_p \mathrm{v}_p}{m_i} \tag{3}$$

$$\mathrm{F}_i^{ext} = \sum_p S_{ip} \mathrm{F}_p^{ext} \tag{4}$$

and i refers to individual nodes of the grid. m_p is the particle mass, $\mathbf{v}_p$ is the particle velocity, and $\boldsymbol{F}_p^{ext}$ is the external force on the particle. S_{ip} is the shape function of the i^{th} node evaluated at x_p.

F^{int} is computed at the nodes as a volume integral of the divergence of the stress on the particles, specifically:

$$\mathrm{F}_i^{int} = \sum_p \mathrm{G}_{ip} \sigma_p v_p \tag{5}$$

where $\mathbf{G}_{ip}$ is the gradient of the shape function of the i^{th} node evaluated at $\boldsymbol{x_p}$, and σ_p and v_p are the time n values of particle stress and volume respectively.

Using Eq. (1) the momentum equations for grid nodes are solved, and then mapped back to the material points. State variables are finally calculated at the material points using the updated kinematic variables.

3. Results and discussion

Two-dimensional simulation model for plastic bonded explosives is shown in Fig. 1. The model was created based on the Voronoi tessellation. It has the same width and length of 10 mm. There are 1024 (32 × 32) HMX grains in total, which contain 939,999 material points. And there are also 60,001 binder points. Considering the density of HMX is 1.9×10^3 kg/m^3 and for binder is 1.1×10^3 kg/m^3, we can get the mass fraction for both constituents is 96.44% and 3.56%, respectively.

An elastic-plastic constitutive-model with a Mie-Gruneisen equation-of-state is used for HMX, and a hyper-elastic constitutive-model is used for binder. The properties for HMX and binder are given in Table 1. Where S_1–S_3 are the coefficients of the slope of the u_s–u_p curve, u_s is shock velocity, and u_p is particle velocity.

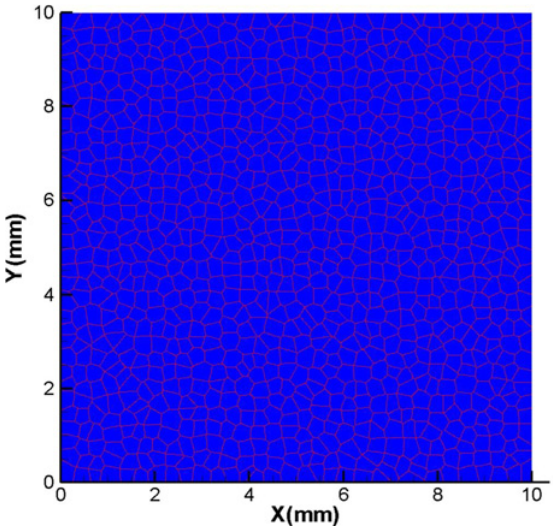

Figure 1. Simulation model for plastic bonded explosive.

Table 1. Parameters for HMX and binder.

	HMX	binder
Density (kg/m^3)	1.90E3	1.10E3
Shear modulus (Pa)	7.20E9	2.70E8
Bulk modulus (Pa)	10.2E9	3.65E9
Yield strength (Pa)	3.70E8	—
Sound speed (m/s)	2901.0	—
Gruneisen gamma	1.1	—
S_1	2.058	—
S_2	0	—
S_3	0	—

3.1. Low shock strength results

Shock loading is performed by a piston moving at a constant velocity from the left boundary to right. The top and bottom boundaries are free slip boundaries. The right boundary is a free surface. In this section, the piston velocity is set to 200 m/s. As shock wave reaches the free surface, the effective stress, plastic strain and temperature distribution of the explosive are shown in Figs. 2–4 (only show the result for HMX grains, not contain the binder).

The results shown in Figs. 2–4 indicate that under shock loading there forms a lot of stress localizations at the interfaces between HMX grains and binder layers. These stress localizations lead to large plastic deformations. Simultaneously, the plastic strain energy transforms to thermal energy, causing the temperature to rise rapidly and form hot spots on grain boundary areas.

3.2. High shock strength results

To increase the shock strength, a higher velocity of 400 m/s for the piston is used. The model properties and other simulation conditions are the same as in Sect. 3.1. The effective stress, plastic strain and temperature distribution

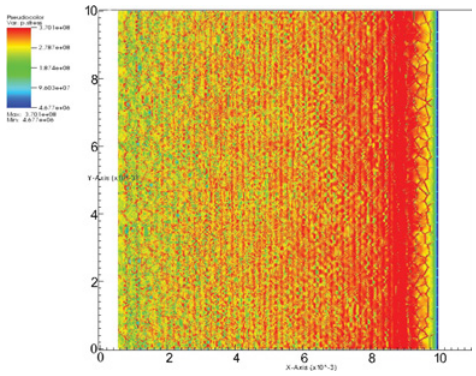

Figure 2. Effective stress distribution for the plastic bonded explosive as shock wave reaches the free surface (piston velocity is 200 m/s).

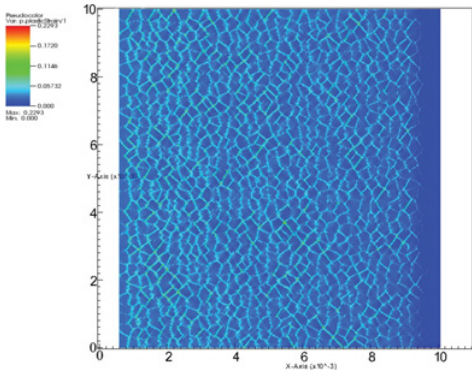

Figure 3. Plastic strain distribution for the plastic bonded explosive as shock wave reaches the free surface (piston velocity is 200 m/s).

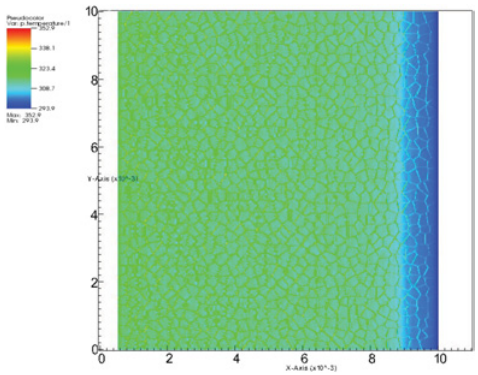

Figure 4. Temperature distribution for the plastic bonded explosive as shock wave reaches the free surface (piston velocity is 200 m/s).

of the explosive as shock wave reaches the free surface are shown in Figs. 5–7 (also only show the result for HMX grains, not contain the binder).

Results shown in Figs. 5–7 indicate that with increasing shock strength, the distributions of stress, plastic strain and temperature do not have significant changes, but their values do have large increases. Thus, a conclusion can be summarized as, the higher the shock strength is, the higher the hot spot temperature will be.

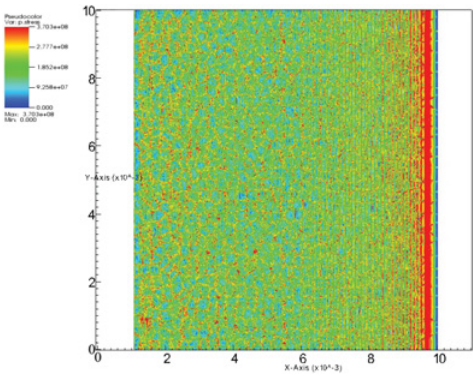

Figure 5. Effective stress distribution for the plastic bonded explosive as shock wave reaches the free surface (piston velocity is 400 m/s).

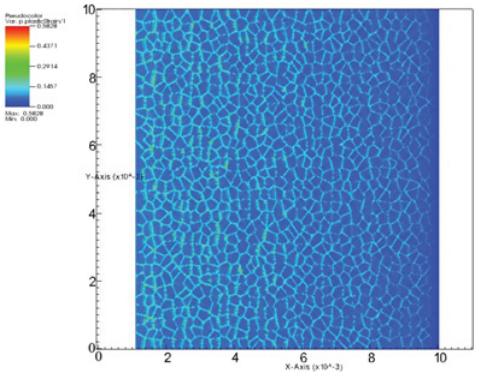

Figure 6. Plastic strain distribution for the plastic bonded explosive as shock wave reaches the free surface (piston velocity is 400 m/s).

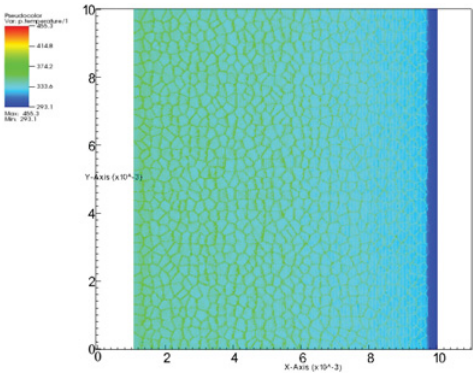

Figure 7. Temperature distribution for the plastic bonded explosive as shock wave reaches the free surface (piston velocity is 400 m/s).

4. Conclusion

In this paper, mesoscale responses of plastic bonded explosives under shock loading are investigated using material point method. Simulation results show that under shock loading there forms a lot of stress localizations at the interfaces between HMX grains and binder layers. And these stress localizations lead to large plastic deformations. Simultaneously, the plastic strain energy transforms to thermal energy, causing the temperature to rise rapidly and form hot spots on grain boundary areas. With increasing shock strength, the distributions of stress, plastic strain and temperature do not have significant changes, but their

values do have large increases. We can conclude that, the higher the shock strength is, the higher the hot spot temperature will be.

This work was supported by National Natural Science Foundation of China (11272296, 11272294), Science and Technology Foundation of CAEP (2014A0201008, 2012A0201007), National Key Laboratory Foundation (2012-Z-05), and Province Programming Foundation of Institute of Fluid Physics (LYGH201402).

References

[1] R. Menikoff, Shock Waves **21**, 141 (2011).
[2] M.R. Baer, Thermochimica Acta **384**, 351 (2002).
[3] P.A. Conley, D.J. Benson, Proceedings of the 11th International Detonation Symposium, 768 (1998).
[4] P. Dickson, B. Asay, B. Henson, L. Smilowitz, Proc. Roy. Soc. Lond. A **460**, 3447 (2004).
[5] D. Sulsky, Z. Chen, H.L. Schreyer, Comput. Methods Appl. Mech. Eng. **118**, 179 (1994).
[6] D. Sulsky, S. Zhou, H.L. Schreyer, Comput. Phys. Commun. **87**, 236 (1995).
[7] F.H. Harlow, Methods Comput. Phys. **3**, 319 (1963).
[8] J.U. Brackbil, H.M. Ruppel, J. Comp. Phys. **65**, 314 (1986).
[9] H.L. Jonah, H. Daisy, IOP Conf. Series: Mater. Sci. Eng. **10**, 012093 (2010).
[10] S.G. Bardenhagen, J.U. Brackbill, D. Sulsky, Comput. Methods Appl. Mech. Eng. **187**, 529 (2000).